Petrological evidence for magma recharge and mixing beneath the Ma'anshan monogenetic volcano of Xiaogulihe in Northeast China

Jian-Qiang Liu, Saskia Erdmann, Li-Hui Chen, Hui-Li Zhang, Bin Wu, Gang Zeng, Xiao-Jun Wang, Zhu-Liang Lei, Xun Yu

Journal Pre-proof

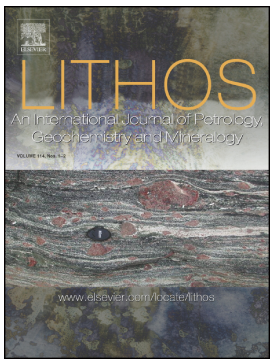

Petrological evidence for magma recharge and mixing beneath the Ma'anshan monogenetic volcano of Xiaogulihe in Northeast China

Jian-Qiang Liu, Saskia Erdmann, Li-Hui Chen, Hui-Li Zhang, Bin Wu, Gang Zeng, Xiao-Jun Wang, Zhu-Liang Lei, Xun Yu

PII: S0024-4937(20)30563-6

DOI: https://doi.org/10.1016/j.lithos.2020.105928

Reference: LITHOS 105928

To appear in: *LITHOS*

Received date: 12 August 2020

Revised date: 6 December 2020

Accepted date: 7 December 2020

Please cite this article as: J.-Q. Liu, S. Erdmann, L.-H. Chen, et al., Petrological evidence for magma recharge and mixing beneath the Ma'anshan monogenetic volcano of Xiaogulihe in Northeast China, *LITHOS* (2020), https://doi.org/10.1016/j.lithos.2020.105928

Petrological evidence for magma recharge and mixing beneath the Ma'anshan monogenetic volcano of Xiaogulihe in Northeast China

Jian-Qiang Liu[1*], Saskia Erdmann[2], Li-Hui Chen[3], Hui-Li Zhang[4], Bin Wu[5], Gang Zeng[4], Xiao-Jun Wang[3], Zhu-Liang Lei[4], Xun Yu[6]

1. Institute of Marine Geology, College of Oceanography, Hohai University, Nanjing 210098, China
2. Université d'Orléans-CNRS/INSU-ISTO-BRGM, UMR 7327, Orléans, France
3. Department of Geology, State Key Laboratory of Continental Dynamics, Northwest University, Xi'an 710069, China
4. State Key Laboratory for Mineral Deposits Research, School of Earth Sciences and Engineering, Nanjing University, Nanjing 210023, China
5. State Key Laboratory of Nuclear Resources and Environment, East China University of Technology, Nanchang 330013, China
6. State Key Laboratory of Marine Geology, Tongji University, Shanghai 200092, China

Corresponding author: Jian-Qiang Liu (liujq@hhu.edu.cn)

Abstract

Geochemical compositions of rocks from monogenetic volcanoes in intraplate settings are commonly used to constrain their mantle source and melting processes; however, the subsequent magmatic evolution of such small-volume volcanic systems is commonly ignored. Here we present petrographic observations, mineral chemistry, whole-rock major and trace element data, and thermodynamic modeling for Quaternary ultrapotassic rocks from the Ma'anshan monogenetic volcano of Xiaogulihe in Northeast China. We use these data to evaluate the crystallization conditions and recharge and mixing processes that the magmas have experienced within the crust. The Ma'anshan volcanic products are predominantly phonotephrite and tephriphonolite. These rocks have small variations in geochemical composition with moderate SiO_2 (47.29–49.4 wt.%), high total alkali contents (K_2O + Na_2O = 9.85–11.87 wt.%), and high K_2O/Na_2O ratios (3.18–4.21). Two types of assemblages were identified in these ultrapotassic rocks: Type-1 antecrysts (olivine and leucite) and hybrid crystals (clinopyroxene, formed by incongruent replacement of antecrysts) and type-2 autocrysts (olivine and leucite). For the type-2, normally zoned olivines, Ni decreases and Mn increases more rapidly with decreasing %Fo than for oceanic basalts, which can be explained by abundant olivine and leucite fractionation in strongly alkaline melts at shallow crustal levels (<200 MPa). The type-1 olivines are reversely zoned and their cores have lower Fo, CaO, and Ni, and higher Mn, than their rims. The type-1 leucites are sieve-textured, partially resorbed, and rimmed by type-1 olivines. The type-1 clinopyroxenes have diopsidic compositions, forming

monomineralic crystal clusters. Although the type-1 antecrystic and hybrid crystals are rare, their presence provides robust evidence for magma recharge and mixing beneath the Ma'anshan monogenetic volcano. This study shows that magmas erupted in monogenetic volcanic fields may experience complex processes within the crust despite their small volumes and relatively uniform compositions, which is important to consider in the interpretation of the construction, evolution, and longevity of their magma plumbing systems.

Keywords: Northeast China; ultrapotassic rocks; Ma'anshan monogenetic volcano; fractional crystallization; magma recharge and mixing.

1. Introduction

Monogenetic volcanic fields (also termed "small-scale basaltic systems") are characterized by clusters of scattered and mostly small (<2 km^2) volcanoes (McGee and Smith, 2016; Németh and Kereszturi, 2015; Smith and Németh, 2017; Walker, 1993). Such volcanic fields are the most widespread form of volcanism on Earth and occur in a variety of different tectonic settings, including intraplate, extensional, and subduction-related environments (Cañón-Tapia, 2016). Due to their small eruptive volumes and entrainment of mantle xenoliths, it is generally considered that magmas erupted in monogenetic volcanic fields have not been significantly modified by magmatic evolution processes (i.e., assimilation and fractional crystallization, or magma recharge and mixing) during their ascent from source to surface (McGee and Smith, 2016; Smith and Németh, 2017). Many geochemical studies have therefore focused on using whole-rock compositions from monogenetic volcanoes to infer the nature of their mantle source(s) and/or degrees of mantle melting (McGee et al., 2012, 2013, 2015a; Rasoazanamparany et al., 2016; Reiners, 2002). Marked correlations have been observed between the volume of individual monogenetic volcanoes and their chemical composition in the Auckland volcanic field, New Zealand, which have been explained by different degrees of melting of a heterogeneous mantle source (McGee et al., 2013, 2015a). In the Auckland volcanic field, nepheline-bearing melts are considered to have originated from a deep, carbonated, garnet peridotite source, whereas less alkalic melts are the products of shallower melting of depleted spinel peridotite (McGee et al., 2015a). However, the bulk composition of erupted rocks

commonly obscures the real details of magmatic evolution, representing the resultant composition of mixed magmas that have experienced different processes and that may comprise different source components. By contrast, high-resolution, mineral-scale textural and chemical investigations can help to unravel the complexity of the magmatic systems feeding monogenetic basaltic volcanoes (Coote et al., 2019; Jankovics et al., 2019; Morgado et al., 2017). A complex set of open- and closed-system processes (including magma stalling, storage, fractionation, mixing, replenishment, cumulate formation and remobilization, incorporation of fragments and crystals from the wall rocks) have been proposed to explain, for example, the various types of olivines and significant compositional variation of olivine-hosted spinel inclusions hosted by the eruptive products of the Fekete-hegy volcanic complex in the intracontinental monogenetic Bakony-Balaton Highland Volcanic Field (Jankovics et al., 2019). Magma residence times in shallow reservoirs obtained via Mg-Fe diffusion modelling in olivine phenocrysts are inferred to vary from a few days to dozens of days for the Caburgua cones of the Andean Southern Volcanic Zone, which indicates the existence of a transient reservoir beneath the small eruptive centers (Morgado et al., 2017).

Numerous geochemical and some petrological studies have been undertaken on Cenozoic volcanic rocks in eastern China that were erupted as monogenetic fields in an intraplate tectonic setting (Fig. 1a), in order to evaluate their mantle source. Five potassium-rich monogenetic volcanic fields (Wudalianchi, Erkeshan, Keluo, Nuominhe, and Xiaogulihe) that are located at the boundary between the northwestern

margin of the Songliao Basin and the Greater Khingan Range (Fig. 1b; Liu et al., 2016, 2017a; Zhang et al., 1998) have been interpreted to derive from metasomatized lithospheric mantle (Chu et al., 2013; Sun et al., 2014; Zhang et al., 1995; Zou et al., 2003) or from recycled ancient sediments from the mantle transition zone (Kuritani et al., 2013; Wang et al., 2017). Previous studies have established that crustal assimilation had played little or no role in their evolution (McGee et al., 2015b; Zou et al., 2003), while the importance of fractionation or magma recharge and mixing remains unconstrained. High-resolution seismic imaging and magnetotelluric studies have identified a significant low-velocity and high-conductivity anomaly at a depth of ~7–13 km below the Weishan volcano of Wudalianchi volcanic field, which is interpreted to delineate a shallow magma storage zone that comprises crystal-rich magma with liquid-rich magma pockets (Li et al., 2016; Zhang et al., 2015). Recently, three-dimensional magnetotelluric imaging further identified a low-resistivity body of 0.3–3.0 Ω·m at depths of ~2–4 km and down to ~15 km beneath the Weishan volcano in the Wudalianchi volcanic field, which corresponds to a magma storage zone in the upper and middle crust. The Weishan volcano is thus likely in an active stage undergoing magma recharge (Gao et al., 2020). This raises the question as to if and under which conditions magmas may have intermittently stalled and evolved at shallow crustal depths beneath K-rich monogenetic volcanoes in Northeast China. The Ma'anshan volcano of Xiaogulihe (Shao et al., 2009) is spatially associated with the Weishan volcano of the Wudalianchi volcanic field (Zhao et al., 2014a) (Fig. 1b). Both volcanoes are characteristic examples of monogenetic volcanoes in Northeast

China that have erupted potassium-rich magmas in the Quaternary (Zhang et al., 1995). In this study, we present detailed petrographic observations, mineral chemical data, whole-rock major and trace element data, and thermodynamic and compositional modelling for Cenozoic ultrapotassic lavas that were erupted at the Ma'anshan monogenetic volcano of Xiaogulihe in Northeast China (Fig. 1c). We use these observations, data, and models to evaluate magma evolution processes in the volcano's crustal magmatic plumbing system.

2. Geological Background

Cenozoic continental intraplate volcanic rocks are widespread in Northeast China, covering an area of ~5000 km^2 (Fig. 1b, Basu et al., 1991; Liu et al., 2001; Zhang et al., 1995). These volcanic rocks are mainly exposed along the flanks of the Songliao Basin with the Greater Khingan Range in the west, the Lesser Khingan Range in the north, and the Changbaishan Mountains in the east (Fig. 1b; He et al., 2019). The Songliao Basin and the Greater Khingan Range are part of the Xing'an–Mongolia Orogenic Belt (XMOB; Fig. 1a), which in turn is the eastern part of the Paleozoic Central Asian Orogenic Belt, which formed during subduction and the collision between the North China Craton and Siberian Plate (Jahn et al., 2000; Sengör et al., 1993). Cenozoic volcanic rocks in Northeast China can be subdivided into ultrapotassic, potassic, and sodic series according to their K_2O contents and K_2O/Na_2O ratios (Liu et al., 2016, 2017a). The potassic (and ultrapotassic) volcanic rocks form about 60 monogenetic volcanoes that are associated with outflows of aa

lavas, which cover an area of >3000 km^2 (Fig. 1b) (Zhao et al., 2014a, 2014b). Based on K–Ar dating, field characteristics and stratigraphy, the volcanic rocks were erupted in three main episodes: in the middle–late Miocene (16.5–7.0 Ma), the late Pliocene to Pleistocene (2.3–0.13 Ma), and the Recent (up to 1721 AD) (Zhang et al., 1998).

3. Sample description

The Ma'anshan monogenetic volcano of Xiaogulihe is located in the northernmost part of the potassic volcanic rock belt in Northeast China (Fig. 1b). Rocks erupted from the Ma'anshan cover an area of about 13.8 km^2 (Fig. 1c). Previous K–Ar dating (0.30–0.19 Ma; Zhang 1992) has shown that the Ma'anshan volcano erupted in the Quaternary, near the end of the second main eruptive episode. In this study, twelve fresh samples were collected from the lava flows of Ma'anshan volcano. The collected samples are porphyritic, massive to vesicular, comprising olivine, leucite, and rare clinopyroxene phenocrysts embedded in a microgranular matrix consisting of leucite, nepheline, sodalite, feldspar, phlogopite, and Fe–Ti oxides (Fig. 2). More detailed petrographic characteristics and mineral chemistry data are presented in the following sections. No mantle-derived xenoliths or xenocrysts were found or have been previously reported in the Xiaogulihe volcanic rocks (Zhang et al., 2000).

4. Analytical Methods

The samples were cut into thin slabs and the fresh central parts were powdered to

~200 mesh for whole-rock geochemical analysis. Whole-rock major element compositions were determined using a Thermo Scientific ARL 9900 X-ray fluorescence (XRF) spectrometer at the State Key Laboratory for Mineral Deposits Research in Nanjing University, Nanjing, China. Based on measured values for standard rock reference materials (BCR-2 and BHVO-2; Wilson, 1997a, 1997b), the analytical accuracy was ±1% for elements with concentrations of >1.0 wt.% and ±10% for elements with concentrations of <1.0 wt.%. Measurements of whole-rock trace element concentrations were undertaken at the Department of Geology, Northwest University, Xi'an, China. Trace elements were determined using an ELAN 6100DRC inductively coupled plasma mass spectrometer (ICP–MS) after acid digestion (HF + HNO_3) of samples in Teflon bombs. Analyses of USGS standards (BHVO-2, AGV-2, and BCR-2; Wilson, 1997a, 1997b, 1998) indicate the precision and accuracy are better than ±5% for Li, Sc, V. Cr, Co, Ni, Cu, Zn, Rb, Sr, Y, Zr, Nb, Ba, Th, and the rare earth elements (REEs), and better than ±10% for Hf, Ta, Pb, and U. Whole-rock major and trace element compositions of twelve Xiaogulihe ultrapotassic rocks and the standard reference materials during the analyses are listed in Table 1 and Table S1 respectively.

We prepared polished thin-sections to characterize the mineral assemblages and textures. Furthermore, several samples were crushed to handpick crystals using a binocular microscope to provide us with a large number of phenocrysts for micro-chemical characterization. Inclusion-rich leucite and clinopyroxene crystals fractured in the process and crucial textural information was lost, and we therefore

exclusively handpicked olivine phenocrysts. Selected olivine grains were mounted in epoxy resin, polished to 0.1 μm, cleaned ultrasonically in ethanol and distilled water, and finally carbon-coated. Major (SiO_2, MgO, and FeO) and minor element (CaO, NiO, and MnO) contents of 441 olivine crystals were acquired in a total of >490 analyses, including core–rim compositions. Major and minor element compositions of 39 leucite and 10 clinopyroxene crystals in thin-sections were also analyzed. All these analyses were undertaken with an electron microprobe (EMP) using a JEOL JXA-8230 Superprobe at the State Key Laboratory of Nuclear Resources and Environment, East China Institute of Technology, Nanchang, China. The beam size was set to 2 μm, and an acceleration voltage of 15 kV and a current of 20 nA were used for all analyses. Calibration standards for the olivine analyses were rhodonite (Si and Mn), magnetite (Fe), olivine (Mg), diopside (Ca), and pentlandite (Ni). Peak counting times were 20 s for major elements (Si, Mg, and Fe), 60 s for minor elements (Ca and Mn), and 90 s for Ni. Background counting times were 5 s on each side of the peaks. To monitor instrumental drift, an internal olivine standard (MongOl; Batanova et al., 2019) was analyzed as an unknown after every five analyses. Seventy-eight analyses of the MongOl olivine showed that the analytical uncertainty was better than ±2% for SiO_2, FeO, and MgO, ±4% for NiO, and ±7% for MnO and CaO. Calibration standards used during the leucite analyses were biotite (Si), rutile (Ti), jadeite (Al and Na), and kaersutite (Fe and K), while those used during the clinopyroxene analyses were almandine garnet (Si), rutile (Ti), jadeite (Al and Na), magnetite (Fe), bustamite (Mn), diopside (Ca, Mg, and Cr), and pentlandite (Ni). Peak counting times were 10 s

and the background counting times were 5 s on each side of the peaks. Analytical uncertainties were <±1% for major elements and <±5% for trace elements. Back-scattered electron (BSE) imaging and electron microprobe X-ray mapping were used to characterize chemical zoning of the minerals. The compositional data for the Xiaogulihe olivines and MongOl olivine standard are provided in Tables S2 and S3 respectively. Major and trace element data for leucite and clinopyroxene are listed in Tables S4 and S5 respectively.

5. Results

5.1 Whole-rock major and trace element compositions

The Xiaogulihe volcanic rocks collected from the Ma'anshan volcano have low SiO_2 (47.29–49.40 wt.%) and high total alkali (K_2O + Na_2O = 9.85–11.87 wt.%) contents, and are mostly phonotephrites and tephriphonolites (Le Bas et al., 1986) (Fig. 3a). The rocks have high K_2O contents (7.83–9.08 wt.%) and K_2O/Na_2O ratios (3.18–4.21), and plot in the field for ultrapotassic rocks (Fig. 3b). Chondrite-normalized rare earth element (REE) patterns reveal that the Xiaogulihe ultrapotassic rocks are enriched in light rare earth elements (LREEs) over heavy rare earth elements (HREEs) (Fig. 4), which are somewhat similar to other potassium-rich rocks from Northeast China.

5.2 Phenocryst textures and compositions

Phenocrysts in the Xiaogulihe ultrapotassic rocks are olivine (10–15 vol.%),

leucite (25 vol.%), and minor clinopyroxene (≤1–2 vol.%) (Fig. 2 and Fig. 5). Based on textures and compositions, we identified two types of phenocryst assemblages (Fig. 5, Fig .6 and Fig. 7). The type-1 assemblages must have crystallized earlier, while the type-2 ones formed later from the magmatic plumbing system. The type-1 olivines (≤ 1–2 vol.% of all olivine crystals) are subhedral to slightly skeletal, and occur as single crystals that are up to ~500 μm in size (Fig. 5a and Fig. 6). The olivines have cores that exhibit irregular resorption surfaces, but the rims are defined by euhedral crystal surfaces (Fig. 6). The type-1 olivines are reversely zoned with cores having lower Fo (76–81), Ni (39–786 ppm), and Ca (1229–1908 ppm), and higher Mn (2726–3516 ppm), than the rims (Fo = 82–87; Ni = 794–1267 ppm; Ca = 1822–2787 ppm; Mn = 1843–2532 ppm; Fig. 5b and Fig. 6). Considering Fe^{2+}–Mg partitioning ($K_D(Fe\text{-}Mg)^{ol\text{-}liq}=0.27\pm0.03$; Draper and Green, 1999), the type-1 olivine core compositions appear to be out of equilibrium with potential host melts, i.e., a melt with a composition equivalent to the bulk rocks (Fig. 8a), and Ni–Ca contents increase and Mn contents decrease with increasing Fo values from core to rim (Fig. 9). The type-2 olivines (>98 vol. % of all olivine crystals) are euhedral–subhedral, up to ~500 μm in size, and occur as single crystals (Fig. 5c and Fig. 7) or crystal clusters (not shown). These olivines are normally zoned and have cores with slightly higher Fo (87–88) and significantly higher Ni (1815–2153 ppm), but lower Ca (1844–2080 ppm) and Mn (1518–1897 ppm) than their rims (Fo = 85–87; Ni = 1037–1391 ppm; Ca = 2151–2887 ppm; Mn = 1758–2440 ppm; Fig. 5d and Fig. 7). Considering Fe^{2+}–Mg partitioning, their core compositions appear to be in equilibrium with a melt

composition that approximates the whole-rock composition (Fig. 8). The more evolved rims of the type-2 crystals appear to have been in equilibrium with the melt that has crystallized to the matrix of the rocks (Fig. 8a). Nickel contents decrease and Ca–Mn contents increase with decreasing Fo content for the type-2 olivines (Fig. 9). However, Ni and Mn contents show a more pronounced decrease and increase with Fo values, respectively, than olivines from Koolau (Hawaii) basalts, mid-ocean ridge basalts (MORB), and high-μ (high $^{238}U/^{204}Pb$, HIMU) ocean island basalts (Fig. 9). The type-2 olivines have compositions and compositional trends that differ entirely from the type-1 crystals, but have similar rim compositions as the type-1 olivines (Fo ~ 86; Fig. 8a and Fig. 9).

The type-1 leucites (≤1–2 vol. % of all leucite crystals) are subhedral, sieve-textured, and up to ~500 μm in size (Fig. 5e). The sieve-textured crystals are filled by fine-grained matrix minerals (ilmenite, clinopyroxene, and apatite), while rimmed by type-1 olivine (Fig. 5e). The type-2 leucites (>98 vol.% of all leucite crystals) are euhedral–subhedral and typically 50–100 μm in size (Fig. 5f). These leucites have relatively homogeneous chemical compositions with ~54.9-57.1 wt.% SiO_2, ~20.0-21.2 wt.% Al_2O_3 and ~21.0-21.9 wt.% K_2O (Table S4). Clinopyroxene phenocrysts (≤1–2 vol.%) in the Ma'anshan volcanic rocks are euhedral–subhedral, up to ~300 μm in size, and form clusters of crystals (Fig. 5g), which we classify as type-1 crystals. They have low Al_2O_3 contents (< 1 wt.%) and Mg# number (83.7-89.2) (Table S5) and plot below the Fe-Mg equilibrium field (Fig. 8b). They are classified as diopside in terms of the nomenclature of Morimoto (1988) (Fig. 5h), and

commonly do not show resorption textures or significant compositional zoning (Fig. 5g).

6. Discussion

6.1 Phenocryst origins

Phenocrysts in volcanic rocks can have a variety of origins (Davidson et al., 2007; Coote et al., 2019). The type-1 and type-2 olivine, leucite, and clinopyroxene phenocrysts may be: (1) Autocrysts that crystallized from and are in equilibrium with the host magma; (2) antecrysts derived from previously crystallized magma pulses in the magmatic plumbing system (Davidson et al., 2007); (3) xenocrysts from crustal or mantle wall-rocks; or (4) hybrid crystals that formed in reactions between the magma and xenocrysts, antecrysts, or autocrysts (Beard et al., 2005; Couch et al., 2001; Erdmann et al., 2012). Crystal textures, zoning, and mineral and host melt compositions are typically used to infer their different origins. All olivine crystals have Fo (76-90%) and NiO (0.005–0.431 wt.%) yet elevated CaO (0.121-0.404 wt.%) contents (Table S2 and Fig. 9), which are unlike those of typical mantle xenocrysts (Foley et al., 2013; Thompson and Gibson, 2000), and clinopyroxene has Al_2O_3 contents of <1.0 wt.% and Mg# < 90 (Table S5), which suggest that none of the crystals are mantle xenocrysts. The euhedral–subhedral morphology and lack of evidence for resorption of the type-2 olivine and leucite crystals (Fig. 5c, Fig. 5f and Fig. 7) indicate an autocrystic origin. Moreover, the cores (~Fo 90) of the type-2 olivine crystals are in Fe–Mg equilibrium with the bulk-rock compositions (Fig. 8a) as

expected for early, near-liquidus crystallization, while the more evolved crystal rims (~Fo 86) are in equilibrium with a melt equivalent to the matrix composition, which is expected for late, pre- or syn-eruptive crystallization, providing further evidence for an autocrystic origin.

In contrast to the type-2 crystals, the type-1 olivine, leucite, and clinopyroxene show clear evidence for textural and/or compositional disequilibrium, indicating an antecrystic, xenocrystic or hybrid origin. The type-1 olivine and leucite occur as single crystals that show evidence for partial resorption (Fig. 5a, Fig. 5e and Fig. 6), which we therefore interpret as antecrysts or crustal xenocrysts. The cores of the type-1 olivines have lower Fo (76-80%) values and NiO (0.005–0.1 wt.%) contents and high MnO (0.352–0.454 wt.%) contents (Fig. 5b and Fig. 6), which are not in equilibrium with their host rock compositions (Fig. 8a). Their compositions are, however, consistent with compositions predicted by fractional crystallization modeling from an initial magma composition equivalent to that of primitive Ma'anshan volcanic rocks (Fig. 9), following extensive crystallization of olivine-leucite-clinopyroxene. We take this as evidence for an antecrystic origin, i.e. we infer that the type-1 crystals formed from a magma batch that crystallized prior to the main Xiaogulihe magmas, and that this early magma batch crystallized to a significant degree. Leucite is rare in crustal rocks, yet it occurred as partially resorbed crystals in the Ma'anshan ultrapotassic magmas, which further argues for an antecrystic and against a crustal xenocrystic origin.

The type-1 clinopyroxenes form monomineralic clusters of relatively small

crystals (Fig. 5g). We rule out that the clinopyroxenes are glomerocrysts (i.e. autocrysts formed by heterogeneous nucleation) or that they formed in a reaction between autocrysts and host melt, as they are out of compositional equilibrium with their host melt (i.e. the composition of the bulk rocks; Fig. 8b). The clinopyroxene crystals could represent antecrysts, e.g. derived from a crystal mush, or they could be hybrid crystals that have formed in a reaction between antecrysts or xenocrysts and host melts (Beard et al., 2005; Couch et al., 2001; Erdmann et al. 2012). We cannot entirely rule out that the clinopyroxene crystals formed after crustal xenocrysts, but we found no evidence for crustal xenocrysts or micro-xenoliths. If the clinopyroxene crystals represented a cluster of antecrysts, we would expect textures indicating partial resorption (as for olivine and leucite), which we do not observe. We favor the interpretation that they have formed in an incongruent reaction between antecrysts and host melt, given that antecrystic olivine and leucite are present (Fig. 5a, 5e and Fig. 6). Hybrid crystals formed in incongruent reactions between antecrysts and melt typically show mono- or poly-mineralic clusters of small, randomly oriented crystals.

6.2 Fractional crystallization in the magmatic plumbing system

We have identified two crystal populations in the Ma'anshan volcanic rocks: (1) Type-1 antecrysts (olivine and leucite) and hybrid crystals (clinopyroxene) that crystallized from previous magma pulses in the magmatic plumbing system; and (2) type-2 autocrysts (olivine and leucite) that crystallized from the main Xiaogulihe magmas. Investigation of the textures and compositions of the various phenocryst

phases can provide conclusive evidence for open-system evolution within the magmatic plumbing system.

For the type-2 olivines, the Ni contents decrease rapidly while the Mn contents increase markedly with decreasing Fo values (Fig. 9). Zhang et al. (2016) reported similar trends for Ni and Mn versus Fo for olivines from the Xiaogulihe volcanic rocks (Fig. 9), and proposed that such compositional trends record variable degrees of mechanical stirring and mixing between different batches of primary melts. However, mixing between relatively Ni-rich and -poor magmas and their olivine populations should produce variably zoned crystals (i.e., abundant crystals that show steep core–rim increases and decreases in Ni), which is not the case. It has been demonstrated experimentally that the olivine/melt partition coefficients for Ni and Mn in strongly alkaline melts ($D_{Ni}^{Ol/Liq}$ = 62–95 and $D_{Mn}^{Ol/Liq}$ = 1.4–2.6) are higher than those in basaltic systems ($D_{Ni}^{Ol/Liq}$ = 2–20 and $D_{Mn}^{Ol/Liq}$ = 0.4–1.8) (Foley and Jenner, 2004). Furthermore, Mn is highly incompatible, and Ni is moderately incompatible in leucite ($D_{Mn}^{Lc/Liq}$ = 0.016 and $D_{Ni}^{Lc/Liq}$ = 0.249) in potassic and ultrapotassic melts (Foley and Jenner, 2004). Thus, fractional crystallization of olivine and leucite from alkaline melts can result in rapid depletion of Ni, but rapid enrichment of Mn, in residual melts (Foley and Jenner, 2004; Foley et al., 2013). Olivine phenocrysts that crystallized from such residual melts would have lower Ni and higher Mn contents, which can explain the steep Xiaogulihe olivine Fo–Ni and Fo–Mn compositional trends (Fig. 9). To test if fractional crystallization of olivine ± clinopyroxene ± leucite could reproduce the observed Ni–Mn–Ca compositional trends (Fig. 9a–c), we

modeled crystallization at 200 MPa using the rhyolite-MELTS software (Gualda et al., 2012; Gualda and Ghiorso, 2015), with the Ni and Mn partition coefficients of Foley and Jenner (2004) and Ca partition coefficient of Herzberg and O'Hara (2002). The modeling results show that the type-2 olivine Ni–Mn–Ca compositions fall on the olivine–leucite liquid line of descent with up to ~13 wt.% olivine and ~25 wt.% leucite crystallization (i.e., at proportions that closely match the observed abundances of type-2 olivine and leucite of 10–15 and ~25 vol.%, respectively; Fig. 9).

As mentioned above, the composition and compositional trends of the Xiaogulihe type-2 olivines differ from those of olivines from oceanic basalts (HIMU, MORBs and Koolau; Fig. 9), which have been interpreted to record extensive fractional crystallization of olivine and leucite in strongly alkaline melts. The difference of absolute Ni, Mn, and Ca contents of olivines at a given Fo value is interpreted to reflect diverse primary magma compositions derived from variably peridotite- or pyroxenite-rich and variably carbonated mantle sources (Herzberg, 2011; Ruprecht and Plank, 2013; Sobolev et al., 2005, 2007). The steep Ni versus Fo compositional trend that is characteristic for the type-2 olivines of Xiaogulihe closely resembles that of Koolau olivines with >Fo89, thus indicating crystallization of similar assemblages and partitioning conditions (for relatively alkali-rich magmas). The shallower Ni versus Fo trend of olivine from MORBs likely reflects the partitioning of Ni between olivine and alkali-poor host melt, as compared to the more alkali-rich Koolau and Xiaogulihe systems. The extensive, shallow Ni versus Fo fractionation trends for olivines from Koolau, HIMU and MORBs with <Fo89 are

characteristic for co-crystallization of olivine, clinopyroxene, and plagioclase (Ruprecht and Plank 2013), as also highlighted by our modelling (which predicts abrupt shallowing of the compositional trend when clinopyroxene joins the crystallizing assemblage; Fig. 9a). The overall relatively flat Ca compositional trends for olivines from Koolau and MORB or the decrease in Ca versus Fo for olivines from HIMU basalts (Fig. 9b) are consistent with extensive plagioclase and/or clinopyroxene co-crystallization, which is characteristic for these rock suites. The steepness of trends of olivine Mn versus Fo increases from MORB over Koolau and HIMU olivine to our type-2 olivine compositional trend, which we infer to reflect an increase in the proportion of co-crystallizing minerals in which Mn is incompatible (i.e. leucite in the Xiaogulihe ultrapotassic rocks).

6.3 Thermodynamic model constraints on phase relations and compositions

To further characterize the phase relations and constrain the crystallization conditions (temperature, pressure, and melt H_2O contents) of the Xiaogulihe ultrapotassic rocks, we undertook thermodynamic modeling using the rhyolite-MELTS software (Gualda et al., 2012; Gualda and Ghiorso, 2015) using the composition of our most primitive Xiaogulihe sample (16XLGH06; MgO = 8.85 wt.%). A range of modeled pressures (50–1200 MPa) and temperatures (900°C–1500°C) were chosen to examine the conditions at crustal depths. Low initial melt H_2O contents (0.5 and 1.0 wt.%) (Chen et al., 2015) and relatively oxidizing conditions (QFM+1) were used as such conditions have previously been inferred for

spatially and temporally associated magma systems (e.g., the Wuchagou, Xunke, and Menluhe volcanic systems; Erdmann et al., 2019; Fig. 1) but also for potassic to ultrapotassic basalts from Eastern China (Hong et al., 2020).

The modeling results indicate that olivine is always the liquidus phase, and crystallizes at ≥1350°C (Fig. 10a, b), which is consistent with the large phenocryst size of type-2 olivine as compared with type-2 leucite (Fig. 5c, 5f). Near-liquidus olivine is modeled to have Fo ~ 89, which matches the observed type-2 olivine core compositions (Fig. 8). For an initial melt H_2O content of 0.5 wt.% and an oxygen fugacity of QFM+1, leucite crystallization is predicted to follow olivine crystallization at 1275°C–1175°C and at pressures of <500–700 MPa (Fig. 10a). At pressures of >500–700 MPa, clinopyroxene is modeled to crystallize after olivine at 1250°C–1175°C, followed by leucite (Fig. 10a). The assemblage of 11–17 vol.% olivine and 16–24 vol.% leucite predicted in the model simulating crystallization at <200 MPa, with an initial melt H_2O content of 0.5 wt.%, provides the best match to the observed phase assemblage and abundance. At higher pressures or melt H_2O contents, olivine, and clinopyroxene become dominant over leucite (Fig. 10a and 10b), which is inconsistent with the mineral proportions observed in the natural samples. Therefore, the co-crystallization of abundant type-2 olivine and leucite, and the absence of autocrystic type-2 clinopyroxene in the Xiaogulihe ultrapotassic rocks, reflect shallow crystallization from a relatively H_2O-poor magma (≤0.5 wt.%) at an oxygen fugacity of ~QFM+1. These constraints suggest that the erupted Xiaogulihe magmas were temporarily stored and partially crystallized at a depth of ~6–7 km,

which is consistent with shallow magma storage that has been imaged geophysically below the Wudalianchi volcanic field (~7–13 km) (Gao et al., 2020; Li et al., 2016). Compared with the Xiaogulihe whole-rock compositional trends, the modeled liquid compositions significantly diverge toward higher SiO_2, Al_2O_3, and TiO_2, and lower MgO and FeO contents (Fig. 10c-10f), indicating that simple fractional crystallization of olivine and leucite alone cannot account for the compositional variation of the Xiaogulihe magmas. Other processes (i.e. magma recharge and mixing) in the magmatic plumbing system may have affected the erupted compositions of the Xiaogulihe magmas.

6.4 Magma recharge and mixing beneath the Xiaogulihe monogenetic volcano

The presence of reversely zoned olivine is commonly taken as evidence for magma recharge and mixing or contamination and partial assimilation of mantle or crustal rocks (Erdmann et al., 2014; Gleeson and Gibson, 2019; Herzberg et al., 2014; Thornber, 2001). Magma recharge and mixing between rift-stored and summit-derived basaltic magmas has been proposed to explain the presence of reversely zoned olivine from Kilauea volcano (Thornber, 2001). Large (>2 mm) reversely zoned olivine crystals in eastern Galápagos basalts have cores with lower Fo contents as compared with their rims, which indicates they record magma recharge and mixing (Gleeson and Gibson, 2019). The cores of type-1 olivines in the Ma'anshan rocks have irregular resorption surfaces, but their rims have planar crystal surfaces and/or euhedral–subhedral crystal habits (Fig. 5a and Fig. 6), which indicate

resorption followed by crystallization. The cores have low Fo (76-80%) and NiO (0.005–0.1 wt.%) contents, and high MnO (0.352–0.454 wt.%) contents (Fig. 9), indicating crystallization from a relatively evolved melt. Our modeling indicates that crystallization of significant amounts of leucite (~40 vol.%), clinopyroxene (~35 vol.%), and olivine (~20 vol.%) at ~200 MPa produces olivine with Ni–Mn–Ca–Fo compositions similar to the type-1 olivine cores (Fig. 9). The core–rim increase in Fo%, Ni, and Ca, and decrease in Mn in the type-1 olivines (Fig. 9) record magma recharge and mixing with a more primitive and/or hotter magma. Thermodynamic modeling (Fig. 9) highlights that the magmas from which the type-1 and type-2 olivine crystallized must have had similar compositions, and that the melt in equilibrium with type-2 olivine was significantly more primitive and hotter than that in equilibrium with type-1 olivine cores. Given that the primitive rims of the type-1 olivines have a relatively narrow width (< 30 μm) compared to the size of the type-2 olivines (Fig. 5a and Fig. 5c), we presume that the type-1 crystals were entrained relatively late during the evolution of the main Ma'anshan magmas (producing only relatively narrow overgrowth zones) when most of the type-2 olivine had already crystallized.

The magma recharge and mixing processes beneath the Ma'anshan monogenetic volcano of Xiaogulihe are further evidenced by the type-1 antecrystic leucite and by the hybrid clinopyroxene crystals. The type-1 leucites are sieve-textured, partially resorbed, and survived as skeletal crystals (Fig. 5f), which indicates that they were at some point not in equilibrium with their host melt. Decompression of

H_2O-undersaturated magmas may cause partial resorption of their crystal cargo and thus lead to the formation of skeletal crystals (Humphreys et al., 2006), but leucite is not predicted to crystallize at large depth (e.g. our model results) and it has also been shown experimentally to be a low-pressure phase (Shea et al., 2009). Furthermore, the type-1 leucites are commonly rimmed by type-2 olivines, which provides evidence for magma recharge and mixing with a more primitive melt. Clinopyroxene clusters in the Xiaogulihe ultrapotassic rocks are interpreted as the hybrid, reaction products between melt and antecrysts or xenocrysts. We favor the interpretation that they formed by reaction between antecrysts and melt, i.e. we suggest that crystal mush fragments were entrained into the hotter recharged magma.

Figure 11 shows a magma recharge and mixing model that can account for the phenocrysts with distinct textures and compositions in the Xiaogulihe ultrapotassic rocks. We suggest that an early shallow magma storage zone existed beneath the Ma'anshan volcano, in which magmas experienced extensive crystallization and formed a crystal-rich mush containing the type-1, low-Fo olivine, leucite, and clinopyroxene (Fig. 11a). Subsequently, this crystal-rich mush was recharged and mixed with a hotter and more primitive magma (Fig. 11b). During this process, the type-1 olivines were partially resorbed, but their planar crystal surfaces and euhedral–subhedral crystal shapes record crystallization of type-2 olivine. The type-1 leucite was also partially resorbed and then overgrown by type-2 olivine. Any clinopyroxene present in the crystal mush (which should have co-existed with the Fo-poor type-1 olivine composition; Fig. 11a) melted during this process, as we have

not identified any antecrystic clinopyroxene crystals. We speculate that the antecrystic clinopyroxene may have been replaced by the hybrid clinopyroxene crystal clusters. Typically, melting of antecrystic clinopyroxenes produces skeletal crystals (e.g. common for plagioclase, where anorthite-rich skeletons partially replace more albite-rich cores, but also observed for other minerals) (Streck, 2008; Erdmann et al., 2014). However, fast dissolution of crystals at conditions outside their stability field (e.g. as for clinopyroxene in the Xiaogulihe magmas, which did not crystallize type-2 autocrysts) could result in complete dissolution of the original crystal(s). During further cooling or decompression of the magmas, they would be supersaturated in nuclei and form new crystals/crystal clusters. Shallow crustal magma storage is inferred to be relatively rare in the plumbing systems beneath monogenetic volcanoes (McGee and Smith, 2016). However, geophysical surveys have suggested that crystal-rich magma mush is present in reservoirs beneath the youngest monogenetic volcanoes of the Wudalianchi volcanic field and that mush-rich zones have completely crystallized beneath older volcanoes at depths of ~3–5 and ~8–15 km (Gao et al., 2020; Li et al., 2016). Our study provides the first direct petrological evidence for the existence of a shallow magma storage zone beneath a K-rich monogenetic volcano in Northeast China. Though petrological studies cannot constrain the architecture of magma plumbing systems as geophysical surveys can, they are crucial for the interpretation of many geological surveys (e.g., by verifying if crustal magma storage zones do indeed exist or if geophysical anomalies correspond to fluid-rich zones) and they are also crucial for their hazard assessment.

7. Conclusions

We used mineral textures, whole-rock, mineral chemical compositions and thermodynamic modeling to investigate the magmatic evolution in the crustal magmatic plumbing system beneath the Ma'anshan volcano in Northeast China. In combination, we interpret our observations and data to indicate that a crystal-rich mush that contained type-1 olivine, leucite, and clinopyroxene had crystallized at shallow level (~200 MPa). The main Xiaogulihe ultrapotassic magmas, which crystallized normally zoned, high-Ni, low-Mn olivine and leucite (type-2) from a low-H_2O melt, recharged and partially mixed with the crystal-rich mush (i.e. a resident magma). The steep decrease in Ni and increase in Mn contents with Fo values of the type-2 olivine record fractional crystallization from alkali-rich melts in which olivine–melt Ni–Mn partition coefficients were high. The presence of some reversely zoned olivines, hybrid clinopyroxene clusters, and partially resorbed leucites overgrown by olivine indicates that the main Xiaogulihe magmas entrained minor volumes (<5 vol.%) of the crystal-rich magma mush. Despite their small eruptive volume and relatively uniform geochemical compositions, magmas erupted in monogenetic volcanic fields may undergo complex magmatic processes in the crust, as shown here for the Xiaogulihe system.

Acknowledgements

We are grateful to Wenli Xie and Ye Liu for their assistance with the major- and

trace-element analyses of the bulk rocks. We also thank Lei Wu for her assistance in mounting olivine in the epoxy targets. We thank Ian E M Smith and two anonymous reviewers for their constructive comments on an earlier version of this manuscript. Lucy McGee and another anonymous reviewer are warmly thanked for their detailed and instructive reviews, and the editorial support of Xian-Hua Li is greatly appreciated. This research was supported by the National Natural Science Foundation of China (41802045 and 41688103), the Fundamental Research Funds for the Central University (Hohai University) (grant 2013/B06414) and the State Key Laboratory for Mineral Deposits Research (Nanjing University) (grant 2018-LAMD-K05). S.E. gratefully acknowledges support from the VOLTAIRE project (ANR-10-LABX-100-01) funded by ANR through the PIA (Programme d'Investissement d'Avenir).

References:

Anders, E. and Grevesse, N., 1989. Abundances of the elements: Meteoritic and solar. Geochimica et Cosmochimica acta, 53(1): 197-214.

Basu, A.R., Wang, J., Huang, W., Xie, G. and Tatsumoto, M., 1991. Major element, REE, and Pb, Nd and Sr isotopic geochemistry of Cenozoic volcanic rocks of eastern China: implications for their origin from suboceanic-type mantle reservoirs. Earth and Planetary Science Letters, 105(1-3): 149-169.

Batanova, V.G., Thompson, J.M., Danyushevsky, L.V., Portnyagin, M.V., Garbe Schönberg, D., Hauri, E., Kimura, J.I., Chang, Q., Senda, R., Goemann, K., Chauvel, C., Campillo, S., Ionov, D.A. and Sobolev, A.V., 2019. New Olivine Reference Material for In Situ Microanalysis. Geostandards and Geoanalytical Research, 43(3): 453-473.

Beard, J.S., Ragland, P.C. and Crawford, M.L., 2005. Reactive bulk assimilation: A model for crust-mantle mixing in silicic magmas. Geology, 33(8): 681-684.

Cañón-Tapia, E., 2016. Reappraisal of the significance of volcanic fields. Journal of Volcanology and Geothermal Research, 310: 26-38.

Chen, H., Xia, Q. and Ingrin, J., 2015. Water content of the Xiaogulihe ultrapotassic volcanic rocks, NE China: implications for the source of the potassium-rich component. Science Bulletin, 60(16): 1468-1470.

Chen, Y., Zhang, Y., Graham, D., Su, S. and Deng, J., 2007. Geochemistry of Cenozoic basalts and mantle xenoliths in Northeast China. Lithos, 96(1-2): 108-126.

Chu, Z., Harvey, J., Liu, C., Guo, J., Wu, F., Tian, W., Zhang, Y. and Yang, Y., 2013. Source of highly potassic basalts in northeast China: Evidence from Re－Os, Sr－Nd－Hf isotopes and PGE geochemistry. Chemical Geology, 357: 52-66.

Coote, A., Shane, P. and Fu, B., 2019. Olivine phenocryst origins and mantle magma sources for monogenetic basalt volcanoes in northern New Zealand from textural, geochemical and δ18O isotope data. Lithos, 344-345: 232-246.

Couch, S., Sparks, R. and Carroll, M.R., 2001. Mineral disequilibrium in lavas explained by convective self-mixing in open magma chambers. Nature, 411(6841): 1037-1039.

Davidson, J.P., Morgan, D.J., Charlier, B.L.A., Harlou, R. and Hora, J.M., 2007. Microsampling and Isotopic Analysis of Igneous Rocks: Implications for the Study of Magmatic Systems. Annual Review of Earth and Planetary Sciences, 35(1): 273-311.

Draper, D.S. and Green, T.H., 1999. P-T phase relations of silicic, alkaline, aluminous liquids: New results and applications to mantle melting and metasomatism. Earth Planetary Science Letters, 170(3): 255-268.

Erdmann, S., Chen, L.H., Liu, J.Q., Xue, X.Q. and Wang, X.J., 2019. Hot, volatile-poor, and oxidized magmatism above the stagnant Pacific plate in Eastern China in the Cenozoic. Geochemistry, Geophysics, Geosystems. 20(11): 4849-4868.

Erdmann, S., Scaillet, B. and Kellett, D.A., 2010. Xenocryst assimilation and formation of peritectic crystals during magma contamination: An experimental study. Journal of Volcanology and Geothermal Research, 198(3-4): 355-367.

Erdmann, S., Scaillet, B. and Kellett, D.A., 2012. Textures of Peritectic Crystals as Guides to Reactive Minerals in Magmatic Systems: New Insights from Melting Experiments. Journal of Petrology, 53(11): 2231-2258.

Erdmann, S., Scaillet, B., Martel, C. and Cadoux, A., 2014. Characteristic Textures of Recrystallized, Peritectic, and Primary Magmatic Olivine in Experimental Samples and Natural Volcanic Rocks. Journal of Petrology, 55(12): 2377-2402.

Fan, Q. and Hooper, P.R., 1991. The Cenozoic basaltic rocks of eastern China: petrology and chemical composition. Journal of petrology, 32(4): 765-810.

Foley, S.F. and Jenner, G.A., 2004. Trace element partitioning in lamproitic magmas—the Gaussberg olivine leucitite. Lithos, 75(1): 19-38.

Foley, S.F., Prelevic, D., Rehfeldt, T. and Jacob, D.E., 2013. Minor and trace elements in olivines as probes into early igneous and mantle melting processes. Earth and Planetary Science Letters, 363: 181-191.

Foley, S.F., Venturelli, G., Green, D.H. and Toscani, L., 1987. The ultrapotassic rocks: characteristics, classification, and constraints for petrogenetic models. Earth-Science Reviews, 24(2): 81-134.

Gao, J., Zhang, H., Zhang, S., Xin, H., Li, Z., Tian, W., Bao, F., Cheng, Z., Jia, X. and Fu, L., 2020. Magma recharging beneath the Weishan volcano of the intraplate Wudalianchi volcanic field, northeast China, implied from 3-D magnetotelluric imaging. Geology. https://doi.org/10.1130/G47531.1.

Gleeson, M.L. and Gibson, S.A., 2019. Crustal controls on apparent mantle pyroxenite signals in ocean-island basalts. Geology, 47(4): 321-324.

Gualda, G.A.R. and Ghiorso, M.S., 2015. MELTS_Excel: AMicrosoft Excel-based MELTS interface for research and teaching of magma properties and evolution. Geochemistry, Geophysics, Geosystems, 16(1): 315-324.

Gualda, G.A., Ghiorso, M.S., Lemons, R.V. and Carley, T.L., 2012. Rhyolite-MELTS: a modified calibration of MELTS optimized for silica-rich, fluid-bearing magmatic systems. Journal of Petrology, 53(5): 875-890.

He, Y., Chen, L.H., Shi, J.H., Zeng, G., Wang, X.J., Xue, X.Q., Zhong, Y., Erdmann, S. and Xie, L.W., 2019. Light Mg isotopic composition in the mantle beyond the Big Mantle Wedge beneath eastern Asia. Journal of Geophysical Research: Solid Earth, 124(8): 8043-8056.

Herzberg, C., 2011. Identification of Source Lithology in the Hawaiian and Canary Islands: Implications for Origins. Journal of Petrology, 52(1): 113-146.

Herzberg, C. and O Hara, M.J., 2002. Plume-associated ultramafic magmas of Phanerozoic age. Journal of Petrology, 43(10): 1857-1883.

Herzberg, C., Cabral, R.A., Jackson, M.G., Vidito, C., Day, J.M.D. and Hauri, E.H., 2014. Phantom Archean crust in Mangaia hotspot lavas and the meaning of heterogeneous mantle. Earth and Planetary Science Letters, 396: 97-106.

Hong, L., Xu, Y., Zhang, L., Wang, Y. and Ma, L., 2020. Recycled carbonate-induced oxidization of the convective mantle beneath Jiaodong, Eastern China. Lithos, 366-367: 105544.

Hsu, C. and Chen, J., 1998. Geochemistry of late Cenozoic basalts from Wudalianchi and Jingpohu areas, Heilongjiang Province, northeast China. Journal of Asian

Earth Sciences, 16(4): 385-405.

Humphreys, M.C., Blundy, J.D. and Sparks, R.S.J., 2006. Magma evolution and open-system processes at Shiveluch Volcano: Insights from phenocryst zoning. Journal of Petrology, 47(12): 2303-2334.

Jahn, B., Wu, F. and Chen, B., 2000. Granitoids of the Central Asian Orogenic Belt and continental growth in the Phanerozoic. Geological Society of America Special Papers, 350: 181-193.

Jankovics, M.É., Sági, T., Astbury, R.L., Petrelli, M., Kiss, B., Ubide, T., Németh, K., Ntaflos, T. and Harangi, S., 2019. Olivine major and trace element compositions coupled with spinel chemistry to unravel the magmatic systems feeding monogenetic basaltic volcanoes. Journal of Volcanology and Geothermal Research, 369: 203-223.

Kress, V.C. and Carmichael, I.S., 1991. The compressibility of silicate liquids containing Fe_2O_3 and the effect of composition, temperature, oxygen fugacity and pressure on their redox states. Contributions to Mineralogy and Petrology, 108(1-2): 82-92.

Kuritani, T., Kimura, J., Ohtani, E., Miyamoto, H. and Furuyama, K., 2013. Transition zone origin of potassic basalts from Wudalianchi volcano, northeast China. Lithos, 156-159: 1-12.

Le Bas, M.J., Le Maitre, R.W., Streckeisen, A. and Zanettin, B., 1986. A chemical classification of volcanic rocks based on the total alkali-silica diagram. Journal of Petrology, 27(3): 745-750.

Li, Z., Ni, S., Zhang, B., Bao, F., Zhang, S., Deng, Y. and Yuen, D.A., 2016. Shallow magma chamber under the Wudalianchi Volcanic Field unveiled by seismic imaging with dense array. Geophysical Research Letters, 43(10): 4954-4961.

Liu, C., Masuda, A. and Xie, G., 1994. Major- and trace-element compositions of Cenozoic basalts in eastern China: Petrogenesis and mantle source. Chemical Geology, 114(1−2): 19-42.

Liu, J., Han, J. and Fyfe, W.S., 2001. Cenozoic episodic volcanism and continental rifting in northeast China and possible link to Japan Sea development as revealed from K−Ar geochronology. Tectonophysics, 339(3 − 4): 385-401.

Liu, J.Q., Chen, L.H., Zeng, G., Wang, X.J., Zhong, Y. and Yu, X., 2016. Lithospheric thickness controlled compositional variations in potassic basalts of Northeast China by melt‐rock interactions. Geophysical Research Letters, 43(6): 2582-2589.

Liu, J.Q., Chen, L.H., Wang, X.J., Zhong, Y., Yu, X., Zeng, G. and Erdmann, S., 2017a. The role of melt‐rock interaction in the formation of Quaternary high‐MgO potassic basalt from the Greater Khingan Range, northeast China. Journal of Geophysical Research: Solid Earth, 122(1): 262-280.

Liu, J.Q., Chen, L.H., Zhong, Y., Lim, W.H. and Wang, X.J., 2017b. Petrological, K-Ar chronological and volcanic geological characteristics of Quaternary Xunke high-Mg# andesites from the Lesser Khingan Range. Acta Petrologica Sinica, 33(1): 31-40.

McGee, L.E., Millet, M., Smith, I.E.M., Németh, K. and Lindsay, J.M., 2012. The

inception and progression of melting in a monogenetic eruption: Motukorea Volcano, the Auckland Volcanic Field, New Zealand. Lithos, 155: 360-374.

McGee, L.E., Smith, I.E.M., Millet, M., Handley, H.K. and Lindsay, J.M., 2013. Asthenospheric Control of Melting Processes in a Monogenetic Basaltic System: a Case Study of the Auckland Volcanic Field, New Zealand. Journal of Petrology, 54(10): 2125-2153.

McGee, L.E., Millet, M., Beier, C., Smith, I.E.M. and Lindsay, J.M., 2015a. Mantle heterogeneity controls on small-volume basaltic volcanism. Geology, 43(6): 551-554.

McGee, L.E., McLeod, C. and Davidson, J.P., 2015b. A spectrum of disequilibrium melting preserved in lava-hosted, partially melted crustal xenoliths from the Wudalianchi volcanic field, NE China. Chemical Geology, 417: 184-199.

McGee, L.E. and Smith, I.E.M., 2016. Interpreting chemical compositions of small-scale basaltic systems: A review. Journal of Volcanology and Geothermal Research, 325: 45-60.

Morgado, E., Parada, M.A., Morgan, D.J., Gutiérrez, F., Castruccio, A. and Contreras, C., 2017. Transient shallow reservoirs beneath small eruptive centres: Constraints from Mg-Fe interdiffusion in olivine. Journal of Volcanology and Geothermal Research, 347: 327-336.

Morimoto, N., 1988. Nomenclature of pyroxenes. Mineralogy and Petrology, 39(1): 55-76.

Németh, K. and Kereszturi, G., 2015. Monogenetic volcanism: personal views and

discussion. International Journal of Earth Sciences, 104(8): 2131-2146.

Putirka, K., 1999. Clinopyroxene+ liquid equilibria to 100 kbar and 2450 K. Contributions to Mineralogy and Petrology, 135(2-3): 151-163.

Rasoazanamparany, C., Widom, E., Siebe, C., Guilbaud, M.N., Spicuzza, M.J., Valley, J.W., Valdez, G. and Salinas, S., 2016. Temporal and compositional evolution of Jorullo volcano, Mexico: Implications for magmatic processes associated with a monogenetic eruption. Chemical Geology, 434: 62-80.

Reiners, P.W., 2002. Temporal-compositional trends in intraplate basalt eruptions: Implications for mantle heterogeneity and melting processes. Geochemistry, Geophysics, Geosystems, 3(2): 1-30.

Ruprecht, P. and Plank, T., 2013. Feeding andesitic eruptions with a high-speed connection from the mantle. Nature, 500(7460): 68-72.

Sengör, A., Natal'In, B.A. and Burtman, V.S., 1993. Evolution of the Altaid tectonic collage and Palaeozoic crustal growth in Eurasia. Nature, 364: 299-307.

Shao, J., Zhang, W., Zhou, X. and Zhang, C., 2009. Discovery of Xiaogulihe perpotassic basic and ultrabasic volcanic rock in the north-west Heilongjiang province, China. Acta Petrologica Sinica, 10(25): 2642-2650.

Shea, T., Larsen, J.F., Gurioli, L., Hammer, J.E., Houghton, B.F. and Cioni, R., 2009. Leucite crystals: Surviving witnesses of magmatic processes preceding the 79AD eruption at Vesuvius, Italy. Earth and Planetary Science Letters, 281(1-2): 88-98.

Smith, I. and Németh, K., 2017. Source to surface model of monogenetic volcanism: a critical review. Geological Society, London, Special Publications, 446(1): 1-28.

Sobolev, A.V., Hofmann, A.W., Sobolev, S.V. and Nikogosian, I.K., 2005. An olivine-free mantle source of Hawaiian shield basalts. Nature, 434(7033): 590-597.

Sobolev, A.V., Hofmann, A.W., Kuzmin, D.V., Yaxley, G.M., Arndt, N.T., Chung, S., Danyushevsky, L.V., Elliott, T., Frey, F.A. and Garcia, M.O., 2007. The amount of recycled crust in sources of mantle-derived melts. Science, 316(5823): 412-417.

Sun, Y., Ying, J., Zhou, X., Shao, J., Chu, Z. and Su, B., 2014. Geochemistry of ultrapotassic volcanic rocks in Xiaogulihe NE China: Implications for the role of ancient subducted sediments. Lithos, 208-209: 53-66.

Thompson, R.N. and Gibson, S.A., 2000. Transient high temperatures in mantle plume heads inferred from magnesian olivines in Phanerozoic picrites. Nature, 407(6803): 502-506.

Thornber, C.R., 2001. Olivine–liquid relations of lava erupted by Kilauea volcano from 1994 to 1998: implications for shallow magmatic processes associated with the ongoing East-Rift-Zone eruption. The Canadian Mineralogist, 39(2): 239-266.

Toplis, M.J. and Carroll, M.R., 1995. An experimental study of the influence of oxygen fugacity on Fe-Ti oxide stability, phase relations, and mineral—melt equilibria in ferro-basaltic systems. Journal of Petrology, 36(5): 1137-1170.

Walker, G.P., 1993. Basaltic-volcano systems. Geological Society, London, Special Publications, 76(1): 3-38.

Wang, X., Chen, L., Hofmann, A.W., Mao, F., Liu, J., Zhong, Y., Xie, L. and Yang, Y., 2017. Mantle transition zone-derived EM1 component beneath NE China: Geochemical evidence from Cenozoic potassic basalts. Earth and Planetary Science Letters, 465: 16-28.

Weiss, Y., Class, C., Goldstein, S.L. and Hanyu, T., 2016. Key new pieces of the HIMU puzzle from olivines and diamond inclusions. Nature, 537(7622): 666-670.

Wilson, S.A., 1997a. The collection, preparation, and testing of USGS reference material BCR-2, Columbia River. Basalt US Geological Survey Open-File Report.

Wilson, S.A., 1997b. Data compilation for USGS reference material BHVO-2, Hawaiian Basalt. US geological survey open-file report: 2-3.

Wilson, S.A., 1998. Data compilation and statistical analysis of intralaboratory results for AGV-2. US Geological Survey Open-File Report: 3.

Zhang, J.B., 1992. Sources characteristics of ultra-potassium basaltic rocks from northeast China and research on regional mantle geochemistry, 3-29 pp, Doctoral dissertation). Beijing, Institute of Geology, Chinese Academy of Sciences.

Zhang, L.Y., Prelević, D., Li, N., Mertz-Kraus, R. and Buhre, S., 2016. Variation of olivine composition in the volcanic rocks in the Songliao basin, NE China: lithosphere control on the origin of the K-rich intraplate mafic lavas. Lithos, 262: 153-168.

Zhang, M., Suddaby, P., O'Reilly, S.Y., Norman, M. and Qiu, J., 2000. Nature of the

lithospheric mantle beneath the eastern part of the Central Asian fold belt: mantle xenolith evidence. Tectonophysics, 328(1−2): 131-156.

Zhang, M., Suddaby, P., Thompson, R.N., Thirlwall, M.F. and Menzies, M.A., 1995. Potassic volcanic rocks in NE China: geochemical constraints on mantle source and magma genesis. Journal of Petrology, 36(5): 1275-1303.

Zhang, M., Zhou, X.H. and Zhang, J.B., 1998. Nature of the lithospheric mantle beneath NE China: evidence from potassic volcanic rocks and mantle xenoliths. In M. F.J. Flower, S-L. Chung, C-H. Lo, and T-Y. Lee (Eds.), Mantle Dynamics and Plate Interactions in East Asia (pp. 197-219). (GEODYNAMICS SERIES; Vol. 27). American Geophysical Union.

Zhang, S.Q., Li, Z.W. and Tian, P.Y., 2015. Integrated study on the geological and geophysical survey in the Wudalainchi Volcano Field, China Geol. Surv. Rep: 1-110.

Zhao, D., Yu, S. and Ohtani, E., 2011. East Asia: seismotectonics, magmatism and mantle dynamics. Journal of Asian Earth Sciences, 40(3): 689-709.

Zhao, Y., Li, N., Fan, Q., Zou, H. and Xu, Y., 2014a. Two episodes of volcanism in the Wudalianchi volcanic belt, NE China: Evidence for tectonic controls on volcanic activities. Journal of Volcanology and Geothermal Research, 285: 170-179.

Zhao, Y., Fan, Q., Zou, H. and Li, N., 2014b. Geochemistry of Quaternary basaltic lavas from the Nuomin volcanic field, Inner Mongolia: Implications for the origin of potassic volcanic rocks in Northeastern China. Lithos, 196-197:

169-180.

Zou, H., Reid, M.R., Liu, Y., Yao, Y., Xu, X. and Fan, Q., 2003. Constraints on the origin of historic potassic basalts from northeast China by U−Th disequilibrium data. Chemical Geology, 200(1-2): 189-201.

Figure Captions

Figure 1. (a) Simplified geological map showing the main tectonic units and spatial distribution of Cenozoic volcanic rocks in eastern China. XMOB = Xing'an–Mongolia Orogenic Belt. The green areas mark the exposure of Cenozoic volcanic rocks in eastern China and the far east of Russia. (b) Geological sketch map modified from He et al. (2019), showing the distribution of sodic and potassic basalts, and high Mg# andesites, in northeast China (Liu et al., 2017a, b; Zhang et al. 1998). Black stippled line indicates the surface expression of the western edge of the present-day stagnant Pacific slab (Zhao et al., 2017). (c) Sketch map showing the occurrence of the Xiaogulihe ultrapotassic basalts around Ma'anshan volcano (modified from Shao et al. (2009)), which cover an area of about 13.8 km^2.

Figure 2. Representative photomicrographs of the Xiaogulihe ultrapotassic rocks. (a) Euhedral leucite and subhedral olivine phenocrysts in sample 16XGLH04; (b) euhedral olivine phenocrysts with crystallized melt inclusions in sample 16XGLH06.

Figure 3. Plots of (a) $Na_2O + K_2O$ versus SiO_2 (Le Bas et al., 1986), and (b) K_2O versus Na_2O for the Xiaogulihe volcanic rocks (red squares) from northeast China. The classification of ultrapotassic, potassic, and sodic series volcanic rocks in K_2O/Na_2O compositional space follows that of Foley et al. (1987). Literature data for the Xiaogulihe ultrapotassic rocks (while squares) are from Sun et al. (2014) and Zhang et al. (2016). Literature data for the Wudalianchi–Erkeshan–Keluo–Nuominhe

potassic rocks (grey triangles) are from Basu et al. (1991), Chen et al. (2007), Chu et al. (2013), Fan and Hooper (1991), Hsu and Chen (1998), Kuritani et al. (2013), Liu et al. (1994), Liu et al. (2017a), Wang et al. (2017), Zhang et al. (1995), Zhao et al. (2014), and Zou et al. (2003).

Figure 4. Chondrite-normalized rare earth element (REE) pattern for the Xiaogulihe ultrapotassic rocks. Literature data for the Xiaogulihe ultrapotassic rocks are from Sun et al. (2014) and Zhang et al. (2016), and those for the Wudalianchi–Erkeshan–Keluo–Nuominhe potassic rocks are from Chen et al. (2007), Chu et al. (2013), Liu et al., (2017a), Wang et al. (2017), Zhao et al. (2014), and Zou et al. (2003). Normalized value of the chondrite is from Anders and Grevesse (1989).

Figure 5. (a) Back-scattered electron (BSE) image and (b) compositional traverses for a type-1 olivine phenocryst from the Xiaogulihe ultrapotassic rocks. The type-1 olivines have cores with lower Fo, NiO, and CaO, and higher MnO, than their rims. (c) BSE image and (d) compositional traverses for a type-2 olivine phenocryst from the Xiaogulihe ultrapotassic rocks. The type-2 olivine cores have higher Fo and NiO, and lower CaO and MnO, than their rims (e) BSE image of a type-1 leucite in sample 16XGLH10. The type-1 leucite contains inclusions of fine-grained matrix minerals (ilmenite, clinopyroxene, and apatite) and is rimmed by the type-2 olivine. (f) BSE image of a type-2 leucite in sample 16XGLH04. (g) BSE image of a type-1 clinopyroxene cluster in sample 16XGLH06. (h) The pyroxene quadrilateral

(Morimoto, 1988) showing the compositions of the type-1 clinopyroxene phenocrysts from the Xiaogulihe ultrapotassic volcanic rocks. Analytical uncertainties are smaller than the symbol size in (b) and (d).

Figure 6. (a) BSE image, (b–c) compositional traverses A–A' and B–B', and (d–f) X-ray elemental maps of a type-1 reversely-zoned olivine from the Xiaogulihe ultrapotassic rocks. The core of this olivine has lower Fo, NiO, and CaO, and higher MnO, than its rim.

Figure 7. (a) BSE image, (b) compositional traverses A-A', and (c-f) X-ray elemental maps of a type-2 normally-zoned olivine from the Xiaogulihe ultrapotassic rocks. The core of this olivine has higher Fo, NiO, and lower CaO and MnO contents, than its rim.

Figure 8. (a) Plot of whole-rock Mg number (Mg#) versus olivine Fo content for the Xiaogulihe ultrapotassic volcanic rocks. We used an equilibrium Fe/Mg olivine–liquid partition coefficient of 0.27 ± 0.03, following Draper and Green (1999), which considers that Fe/Mg partitioning varies with the alkali content of a melt. Melt FeO and Fe_2O_3 contents were estimated using the eq. 7 of Kress and Carmichael (1991) at fO_2 = QFM+1, 200 MPa, and 1350°C. Arrows indicate the relative effects of xenocryst addition (upward), crystal accumulation (rightward), and groundmass crystallization or evolved trends (downward) on equilibrium Fe/Mg compositions. (b)

Whole-rock Mg# versus Mg# of clinopyroxene grains. The Fe-Mg exchange partition coefficient between clinopyroxene and basaltic melt falls from 0.27 (Putirka, 1999) to 0.23 (Toplis and Carroll, 1995).

Figure 9. Plots of (a) Ni, (b) Ca, and (c) Mn versus Fo values for the type-1 and -2 olivines in the Xiaogulihe ultrapotassic volcanic rocks. Also shown for comparison are the previously published compositional fields for olivines from the Xiaogulihe rocks (Zhang et al., 2016), olivine compositions from MORBs, Koolau (Sobolev et al., 2007), and HIMU basalts (Weiss et al., 2016). Black solid fields represent calculated Ni, Ca, and Mn contents for olivines crystallized from primary melts derived from a fertile peridotite source (Herzberg, 2011). Dotted black curves delineate compositional trends for modeled olivines along a possible liquid line of descent (LLD) from sample 16XGLH06 at 200 MPa. We calculated the LLD for the K-rich magma system using the rhyolite-MELTS software of Gualda and Ghiorso (2015) for crystallization at relatively oxidizing conditions (QFM+1) and at low H_2O content (0.5 wt.%). The composition of olivines that crystallized along the LLD were calculated using partition coefficients reported by Foley and Jenner (2004) (Ni and Mn) and Herzberg and O'Hara (2002) (Ca). Gray dotted lines indicate the compositional trends inferred to record recharge and mixing between magmas containing the type-1 and type-2 olivines.

Figure 10. Summary of selected thermodynamic model results for sample

16XLGH06. (a–b) Predicted phase relations for the Xiaogulihe magmas assuming initial H_2O contents of 0.5 and 1.0 wt.% at QFM+1. Phases are labeled within their stability fields. Ol = olivine; Lc = leucite; Cpx = clinopyroxene; Ap = apatite; Ox = oxides; Kfs = K-feldspar. (c) SiO_2 versus TiO_2, (d) SiO_2 versus Al_2O_3, (e) SiO_2 versus Fe_2O_3 and (f) SiO_2 versus MgO for modeled liquid compositions and whole-rock composition of Xiaogulihe ultrapotassic rocks.

Figure 11. Schematic diagrams showing our magma recharge and mixing model beneath the Ma'anshan monogenetic volcano of Xiaogulihe. We suggest that a shallow, mushy magma storage zone existed beneath the Ma'anshan volcano, (a). This zone was recharged by a hotter and more primitive magma (b). During magma recharge and mixing, type-1 olivine and leucite were partially resorbed and then partially overgrown by type-2 olivine. Clinopyroxene antecrysts (if initially present) did not survive this process, but may have reacted with the liquid of the main magma to form hybrid crystal clusters with a relatively Mg-rich composition, in near-equilibrium with the host melt.

Declaration of interests

☒ The authors declare that they have no known competing financial interests or personal relationships that could have appeared to influence the work reported in this paper.

☐The authors declare the following financial interests/personal relationships which may be considered as potential competing interests:

Table 1 Whole-rock major element (wt.%) and trace element compositions (ppm) of Xiaogulihe ultrapotassic rocks in N

Sample	16XGLH01	16XGLH02	16XGLH03	16XGLH04	16XGLH05	16XGLH06	16XGLH07	16XGLH08	16XGLH09
	N50°44′50.6″ E 124°47′50.9″				N 50°44′49.6″ E 124°47′32.3″	N 50°44′44.5″ E 124°47′21″	N 50°44′34.9″ E 124°47′9.03″	N 50°43′28.3″ E 124°46′26.9″	N 50°42′46.5″ E 124°44′38.3″
SiO_2	48.39	48.38	49.40	47.66	48.00	47.36	48.04	48.26	49.01
TiO_2	2.90	2.96	3.01	2.92	2.91	2.82	2.86	3.02	3.03
Al_2O_3	11.10	11.17	11.56	11.17	11.30	11.29	11.26	11.40	11.59
Fe_2O_3t[a]	7.60	7.66	7.80	7.60	7.70	7.94	7.91	7.74	7.47
MnO	0.11	0.11	0.12	0.11	0.11	0.11	0.11	0.12	0.11
MgO	8.23	8.29	8.34	8.33	8.40	8.85	8.97	8.13	7.61
CaO	6.12	6.05	6.33	6.39	6.33	6.67	6.46	6.15	5.60
Na_2O	2.02	2.51	2.42	2.22	2.60	2.40	2.01	1.97	2.56
K_2O	8.50	8.50	8.57	8.05	8.26	7.85	7.98	7.88	8.91
P_2O_5	1.12	1.22	1.72	1.64	1.67	1.72	1.17	1.72	1.43
LOI[b]	2.55	1.88	1.60	2.60	1.39	1.55	1.79	2.17	1.37
Total	98.64	98.73	100.86	98.70	98.67	98.55	98.56	98.56	98.69
Mg#[c]	70.45	70.44	70.18	70.70	70.60	71.05	71.40	69.81	69.16
Li	6.84	7.27	7.15	7.18	7.33	6.72	7.45	6.68	7.41
Be	7.46	7.75	7.65	7.53	7.48	6.29	6.80	7.69	7.02
Sc	18.1	18.6	18.5	18.2	18.4	18.0	18.2	18.4	17.6
V	122	113	149	154	153	158	172	159	146
Cr	240	245	241	238	250	269	267	232	217
Co	34.1	34.4	33.4	35.5	34.4	37.5	36.6	32.7	31.2
Ni	202	205	193	199	197	213	213	191	187
Cu	38.9	36.9	34.3	35.1	36.5	37.9	37.5	32.3	34.8
Zn	98.8	100.6	99.1	97.6	98.7	96.9	97.8	99.1	98.6
Ga	25.3	25.9	25.8	25.1	25.1	23.6	24.3	25.6	25.6
Ge	1.75	1.78	1.75	1.72	1.68	1.59	1.66	1.75	1.74
Rb	152	152	159	163	147	140	144	176	156
Sr	1175	1143	1461	1593	1565	1622	1249	1481	1267
Y	26.0	25.2	26.6	25.9	26.4	24.5	25.2	26.5	25.4
Zr	904	925	916	900	884	749	817	915	844
Nb	70.7	72.6	72.1	70.5	70.7	69.1	71.3	70.6	69.0
Cs	1.39	1.40	1.42	1.39	1.36	1.30	1.35	1.46	1.36
Ba	3568	3835	2106	3182	3259	3131	3739	2322	2912
La	154	157	158	154	156	137	145	156	152
Ce	311	316	317	307	309	273	285	316	305
Pr	34.0	34.7	35.0	33.9	34.2	30.0	31.5	35.1	33.9
Nd	126	130	130	127	127	112	118	129	126
Sm	17.5	17.9	18.0	17.5	17.7	15.7	16.4	18.1	17.4
Eu	4.45	4.57	4.47	4.44	4.48	4.05	4.27	4.51	4.39
Gd	12.9	13.1	13.2	12.9	13.1	11.7	12.3	13.2	12.8
Tb	1.35	1.38	1.39	1.35	1.38	1.26	1.30	1.38	1.33
Dy	6.21	6.31	6.37	6.21	6.33	5.85	6.03	6.39	6.13

Ho	0.94	0.96	0.97	0.95	0.97	0.90	0.93	0.97	0.92
Er	2.33	2.36	2.40	2.34	2.40	2.21	2.26	2.38	2.27
Tm	0.28	0.28	0.29	0.28	0.28	0.26	0.27	0.28	0.27
Yb	1.56	1.59	1.61	1.55	1.62	1.50	1.54	1.60	1.51
Lu	0.22	0.22	0.22	0.21	0.22	0.20	0.21	0.22	0.21
Hf	22.1	22.9	22.7	22.1	21.7	18.4	20.1	22.8	20.9
Ta	3.65	3.77	3.77	3.67	3.56	3.72	3.78	3.71	3.69
Pb	36.1	36.6	37.4	36.6	18.1	27.3	34.5	37.3	26.3
Th	8.08	8.28	8.38	8.16	8.35	7.75	8.05	8.31	7.63
U	1.60	1.81	1.70	1.61	1.74	1.60	1.63	1.69	1.66

[a] $Fe_2O_3^t$, total iron as Fe_2O_3.

[b] LOI=Loss on ignition.

[c] $Mg\#=Mg^{2+}/(Mg^{2+}+Fe^{2+})$, assuming $Fe^{3+}/Fe_{total} = 0.1$, cation ratio.

Highlights:

1. First petrological evidence for complex magma processes beneath Ma'anshan volcano
2. Magma mixing and recharge in a monogenetic volcanic system
3. Compositions and texture of antecrysts record magma recharge and mixing